The Future Climate Change Projections for the Hengduan Mountain Region Based on CMIP6 Models

Cuihua Bian , Xinlan Liang * , Bingchang Li , Zhiqiang Hu , Xiaofan Min , Zihao Yue

Posted Date: 28 April 2025

doi: 10.20944/preprints202504.2301.v1

Keywords: CMIP6 Models; Hengduan Mountain Region; Climate Change; Model Evaluation; Emission Scenarios

 doi:10.20944/preprints202504.2301.v1

Article

The Future Climate Change Projections for the Hengduan Mountain Region Based on CMIP6 Models

Cuihua Bian, Xinlan Liang *, Bingchang Li, Zhiqiang Hu, Xiaofan Min and Zihao Yue

College of Water Conservancy and Hydropower Engineering, Sichuan Agricultural University, Ya'an625014,China;202206291@stu.sicau.edu.cn(C.B.); libingchang@stu.sicau.edu.cn (B.L.); huzhiqang1@stu.sicau.edu.cn(Z.H.); minxiaofan@stu.sicau.edu.cn(X.M.); yuezihao@stu.sicau.edu.cn(Z.Y.)

* Correspondence: liangxinlan@sicau.edu.cn

Abstract: In the context of global climate change, there is a lack of research quantifying the uncertainty of mountain ecosystems in relation to the CMIP6 multi-model ensemble simulations. This study aims to assess the future temperature and precipitation trends in the Hengduan Mountains under global climate change and quantify the uncertainty of CMIP6 multi-model ensemble simulations. Based on data from 11 CMIP6 climate models, the study uses bilinear interpolation to standardize model resolution, employs inverse distance weighting interpolation to analyze spatial distribution characteristics, and applies the multi-model ensemble mean method to reduce systematic biases. Through an equal-weight model selection method, EC-Earth3-Veg and MPI-ESM1-2-HR were identified as the optimal model combination. The research findings indicate: (1) During the reference period (1985–2014), the model simulations exhibit systematic biases, with simulated temperature values being 0.46 ± 0.08 °C/month lower and simulated precipitation values 2.07 ± 0.32 mm/month higher than the observations. (2) For the future period (2031–2070), the projected regional warming rates in typical years under the SSP1-2.6, SSP2-4.5, and SSP5-8.5 scenarios are −0.294 ± 0.021°C/decade, 0.081 ± 0.009 °C/decade, and 0.171 ± 0.012 °C/decade, respectively. (3) Precipitation exhibits an overall decreasing trend, with the most pronounced decline under the SSP5-8.5 scenario (−0.68 ± 0.07%). This study is the first to systematically quantify the uncertainty of CMIP6 models in the Hengduan Mountains, revealing the regional climate change trends, provides scientific basis for developing adaptive strategies, and identifies key paths for improving regional climate models.

Keywords: CMIP6 Models; Hengduan Mountain Region; Climate Change; Model Evaluation; Emission Scenarios

1. Introduction

In the context of global climate change, mountain ecosystems have emerged as critical regions for investigating climatic impacts and responses due to their distinctive geographical characteristics and heightened climate sensitivity [1,2]. These ecosystems not only serve as habitats for numerous rare and endemic species but also function as essential water conservation zones, playing a pivotal role in maintaining global ecological equilibrium and facilitating sustainable human development. However, climate change is profoundly destabilizing mountain ecosystems [3]. As global warming progresses, sustained temperature elevation and precipitation pattern alterations have induced dramatic ecological shifts. High-altitude plant communities in the Himalayan range are migrating upward at a rate of 27 meters per decade, resulting in approximately 90% of endemic species modifying their elevational range boundaries [4]. Concurrently, the Ganges-Brahmaputra-Meghna basin is experiencing a total water storage reduction of 12.2 ± 3.4 cubic kilometers annually, compromising water security for over 500 million inhabitants [5]. Furthermore, permafrost

 doi:10.20944/preprints202504.2301.v1

degradation has diminished slope stability, exacerbating geological hazards and impeding regional socioeconomic development [6]. These phenomena have precipitated complex environmental responses, including ecosystem transitions, water resource security restructuring, and intensified geological risk profiles, collectively presenting multidimensional and compound challenges to regional sustainability [7]. Such manifestations comprehensively illustrate the vulnerability and sensitivity of mountain ecosystems to climate change dynamics.

Climate system models, as core tools for studying the mechanisms of climate change and predicting future trends, reflect the continuous deepening of human understanding of the climate system [8–11]. Particularly, the innovations introduced by CMIP6 have provided unprecedented opportunities for studying climate change in regions with complex topography [12,13]. In recent years, CMIP6 models have demonstrated high reliability in simulating the climate of complex terrain regions, and thus have been widely applied in mountain climate modeling [14–18]. Based on this, applying these models to the Hengduan Mountains, which also have complex topography, is expected to provide reliable scientific evidence for climate change research in this region. As a crucial component of global mountain ecosystems, the Hengduan Mountains not only share common characteristics in terms of mountain ecosystems' responses to climate change, but also exhibit unique regional features due to their location at the transitional zone between the Tibetan Plateau, the Yunnan-Guizhou Plateau, and the Sichuan Basin. The area is characterized by a complex terrain consisting of plateaus, gorges, and basins, along with diverse climate conditions [19–21]. Previous studies have shown that the Hengduan Mountains are experiencing a significant "warming and drying" trend, with a warming rate of 0.16°C per decade and a precipitation decrease of 11.41 mm per decade [22]. However, it remains unclear whether these changes are consistent with the simulations from CMIP6 models. Although some studies have analyzed temperature and precipitation changes in the Hengduan Mountains using satellite remote sensing data and ground-based observations [23,24], systematic evaluations of the applicability and simulation accuracy of CMIP6 models in this region are still lacking. Therefore, applying CMIP6 models to study climate change in the Hengduan Mountains is of significant importance. Furthermore, existing research has mostly focused on changes in single climate factors [25,26], and a comprehensive and in-depth understanding of the combined impacts of topography, climate, and anthropogenic factors on climate change has not yet been formed. In particular, the trends and uncertainties of future climate change in the Hengduan Mountains under different socio-economic scenarios remain to be further studied and discussed.

Addressing the aforementioned research deficiencies, this investigation employs CMIP6 models in conjunction with high-resolution topographical data and multi-model ensemble averaging methodologies to systematically evaluate CMIP6 model performance in the Hengduan Mountains region. Through comparative analysis between model projections and observational data, this study comprehensively examines future temperature and precipitation trends in the Hengduan Mountains and explores interaction mechanisms among topographical features, climatic factors, and anthropogenic influences in regional climate change dynamics. The findings aim to provide scientific foundations for ecological environmental protection, water resource management, and climate change policy formulation in the Hengduan Mountains, thereby facilitating sustainable development initiatives in this critical region.

2. Data and Methods

2.1. Overview of the Study Area

The Hengduan Mountains are situated in southwestern China, constituting a critical transitional zone connecting the first and second topographical steps of China's terrain. Due to divergent research objectives and thematic focuses among scholars, the spatial delineation of this region lacks standardized boundaries [27–30]. In the present study, after comprehensive consideration of both climatic and topographical factors influencing regional climate dynamics, the Hengduan Mountains

 doi:10.20944/preprints202504.2301.v1

region is defined as encompassing the area between 24°30′–33°43′ N latitude and 97°20′–104°25′ E longitude.

This region is characterized by an intricate interlacement of mountain ranges and hydrological systems, manifesting a distinctive configuration of "seven mountain ranges" (Minshan, Qionglai, Daxueshan, Shaluli, Mangkang-Yunling, Taniantaweng-Nushan, and Boshula-Gaoligong) and "six rivers" (Minjiang, Daduhe, Yalongjiang, Jinshajiang, Lancangjiang, and Nujiang). The Hengduan Mountains epitomize a quintessential monsoon climate region, where monsoon systems interact with complex topography to sculpt pronounced seasonal and altitudinal climatic gradients. From a geological perspective, this region is positioned within the collision and compression zone between the Eurasian and Indian Ocean plates, exhibiting alternating high mountains and deep valleys, well-developed fault structures, active neotectonic movements, and dramatic topographical relief. This topographical configuration compels warm, humid air currents to ascend during their progression, thereby generating complex precipitation distribution patterns and exerting a decisive influence on regional climate dynamics.

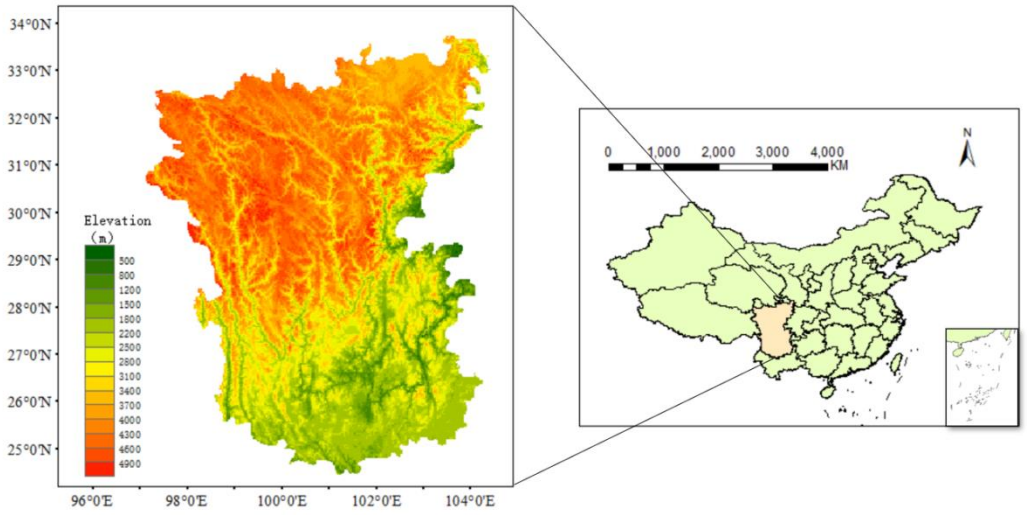

Figure 1. Map of the Hengduan Mountain Region Location.

2.2. Data and Methods

2.2.1. CMIP6 Model Data

Based on data accessibility considerations and informed by precedent investigations [31,32], this study ultimately selected 11 CMIP6 global climate models that have demonstrated superior performance in simulating Chinese precipitation and temperature patterns (Table 1). These models have exhibited distinctive advantages in climate simulation studies across various mountainous regions, thereby providing robust data support and methodological references for comprehensive exploration of climate change dynamics in the Hengduan Mountains region.

Table 1. Basic Information of the 11 Climate Models.

Number	Model Name	Spatial Resolution	Institution	Selection Criteria
1	ACCESS-CM2	288×180	CSIRO	Accurately simulate temperature and precipitation in mountainous and high-altitude regions around Australia, capturing the local climatic characteristics of complex terrains.
2	ACCESS-ESM1-5	512×256	CSIRO	

 doi:10.20944/preprints202504.2301.v1

3	BCC-CSM2-MR	384×192	BCC	Excellently simulate the mean climate and inter-annual variability in regions like China's Qilian Mountains, capturing circulation and precipitation patterns.
4	CanESM5	320×160	CCCma	High-precision simulation of climate in mountainous regions such as the Canadian Rockies, reflecting the impact of mountains on airflow, temperature, and precipitation.
5	EC-Earth3	192×145	EC-Earth-Consortium	Accurately represent the microclimate of mountainous regions such as the European Alps, taking into account vegetation-climate interactions.
6	EC-Earth3-Veg	512×256	EC-Earth-Consortium	
7	FGOALS-f3-L	192×144	CAS	Accurately simulate the thermal and dynamic effects of regions such as the Tibetan Plateau, reflecting the influence of topography on atmospheric circulation.
8	INM-CM4-8	128×64	INM	Precisely simulate long-term trends in temperature and precipitation in Russian mountainous regions, capturing internal variability within the climate system.
9	INM-CM5-0	192×144	INM	
10	KACE-1-0-G	180×120	NIMS-KMA	Effectively simulate meso-scale and micro-scale weather and local climate in mountainous regions such as the Taebaek Mountains in South Korea, capturing extreme weather events.
11	MPI-ESM1-2-HR	180×120	MPI-M	Excellently simulate the climate in regions with complex terrains such as the European Alps, meticulously depicting the influence of topography on climate.

The aforementioned model data were obtained from the Earth System Grid Federation repository (https://esgf-node.ipsl.upmc.fr/search/cmip6-ipsl/), encompassing temperature and precipitation simulation data from historical climate experiments covering the period 1985-2014, as well as climate projections for 2031-2070 under three distinct future scenarios: SSP1-2.6 (sustainability-focused development with low radiative forcing), SSP2-4.5 (middle-of-the-road development with moderate radiative forcing), and SSP5-8.5 (fossil fuel-driven development with high radiative forcing).

2.2.2. Bilinear Interpolation Method

Bilinear interpolation, as a canonical algorithm for two-dimensional spatial data interpolation, finds extensive application across multiple disciplines including geographic information science and meteorology. Its fundamental principle is predicated on linear interpolation concepts, utilizing known discrete data points to estimate values at unknown locations. To illustrate, consider a 2×2 grid with four vertices A, B, C, and D, corresponding to known values f(A), f(B), f(C), and f(D), where the objective is to determine the value at an unknown point P within the grid.

Initially, linear interpolation is performed in the horizontal direction:

First, linear interpolation is performed in the horizontal direction:

Along the edge AB, the function value at point P is:

 doi:10.20944/preprints202504.2301.v1

$$f(P_1) = \frac{x_2 - x}{x_2 - x_1} f(A) + \frac{x - x_1}{x_2 - x_1} f(B) \quad (1)$$

Along the edge CD, the function value at point P is:

$$f(P_1) = \frac{x_2 - x}{x_2 - x_1} f(D) + \frac{x - x_1}{x_2 - x_1} f(C) \quad (2)$$

where x is the horizontal coordinate of point P, x_1 and x_2 are the horizontal coordinates of points A, B (or D, C), respectively.

Then, linear interpolation is performed vertically on P1 and P2 to obtain the function value at point P:

$$f(P) = \frac{y_2 - y}{y_2 - y_1} f(P_1) + \frac{y - y_1}{y_2 - y_1} f(P_2) \quad (3)$$

where y is the vertical coordinate of point P, y_1 and y_2 are the vertical coordinates of points A, D (or B, C), respectively.

In the present investigation, considering the relatively coarse and heterogeneous resolutions of the 11 selected CMIP6 models, bilinear interpolation was employed to resample climate model data onto a 0.5°×0.5° grid to facilitate effective comparison between model simulations and observational measurements, thereby ensuring data consistency and comparability. Bilinear interpolation was selected for its algorithmic elegance, computational efficiency, capacity to maintain first-order continuity, and ability to generate smoothly interpolated outcomes.

2.2.3. Inverse Distance Weighting (IDW) Interpolation Method

The Inverse Distance Weighting (IDW) interpolation method operates on the principle of inverse proportionality to distance, fundamentally postulating that unknown points in closer proximity to known data points are more significantly influenced by those known points. In practical applications, given n known data points with corresponding function values, the value z at an unknown point P can be calculated using the following formula:

$$Z = \frac{\sum_{i=1}^{n} \frac{z_i}{d_i^p}}{\sum_{i=1}^{n} \frac{1}{d_i^p}} \quad (4)$$

where in $d_i = \sqrt{(x - x_i)^2 + (y - y_i)^2}$ represents the distance from the unknown point P to known points, and P denotes a power parameter exceeding 0, conventionally assigned values of 1 or 2. As the P value increases, the influence of distance becomes more pronounced, resulting in heightened contributions from proximal known data points to the interpolation result at unknown points.

In this investigation, the IDW interpolation method was implemented within a Geographic Information System (GIS) platform to spatially interpolate temperature and precipitation variation data across the Hengduan Mountains, facilitating comprehensive analysis of their spatial distribution characteristics. The methodological advantages of IDW interpolation lie in its capacity to thoroughly account for distance relationships between data points, rendering it particularly suitable for interpolating spatially heterogeneous data. By appropriately weighting distances, the IDW interpolation method effectively mitigates interpolation biases attributable to non-uniform data point distribution, thereby more accurately reflecting spatial variation trends in temperature and precipitation across the Hengduan Mountains region and establishing a reliable data foundation for subsequent climate change analyses.

2.2.4. Multi-Model Ensemble (MME)

Climate numerical models constitute fundamental instruments for investigating regional climate change dynamics; however, their inherent systematic biases (such as parameterization scheme deficiencies) and initial field uncertainties may engender significant errors in projections derived from individual models. To mitigate the interference of such uncertainties in climate impact

 doi:10.20944/preprints202504.2301.v1

assessments, this study implements the Multi-Model Ensemble (MME) approach, which integrates outputs from multiple models and synergistically utilizes independent information from each model to enhance simulation robustness and reliability. This methodology has been extensively validated for its efficacy in reducing single-model biases and improving capabilities to capture regional climate characteristics [33].

The investigation adheres to the World Meteorological Organization (WMO) seasonal classification standards, defining March-May, June-August, September-November, and December-February as spring, summer, autumn, and winter respectively, thereby ensuring temporal consistency in climate analyses.

2.2.5. Data and Model Selection

This investigation employs daily temperature and precipitation data from global meteorological stations published by the National Centers for Environmental Information (NCEI), operating under the National Oceanic and Atmospheric Administration (NOAA) (accessible at: https://www.ncei.noaa.gov/), to systematically evaluate the historical simulation performance of 11 CMIP6 models. Utilizing data from the baseline period 1985–2014, quantification of model biases in temperature and precipitation simulations is achieved through comparative analysis between model outputs and continuous observational sequences from 21 ground-based meteorological stations, whose spatial distribution encompasses the principal geomorphological units of the Hengduan Mountains region.

2.2.6. Ensemble Strategy and Threshold Setting

To optimize model selection for future climate projections, the following statistical thresholds were established:

For temperature evaluation: Models exhibiting biases beyond ±1 standard deviation (±0.628 °C/month) of the multi-model mean bias were excluded as low-performance models;

For precipitation assessment: A more stringent threshold of ±0.5 standard deviation (±1.034 mm/month) was implemented to mitigate the systematic overestimation commonly observed in precipitation simulations (as elaborated in Section 3.1).

The optimally selected models (EC-Earth3-Veg and MPI-ESM1-2-HR) were subsequently integrated through Equal-Weighted Ensemble methodology to generate a Multi-Model Ensemble (MME) dataset. This approach not only equilibrates contributions from individual models but also significantly enhances the signal-to-noise ratio of projection results through variance reduction [34]. Utilizing the MME dataset, spatio-temporal evolution characteristics of temperature and precipitation in the Hengduan Mountains region during 2031–2070 were further analyzed under SSP1-2.6, SSP2-4.5, and SSP5-8.5 scenarios.

3. Results and Analysis

3.1. Current Climate Analysis

3.1.1. Spatial Distribution Characteristics of Temperature and Precipitation

Given that CMIP6 historical experiments terminate at the 2014 chronological boundary, the period 1985–2014 was established as the reference baseline for comparative analysis of seasonal spatial variations between observational data from NOAA (OBS) and the multi-model ensemble average (MME) derived from 11 models (as illustrated in Figure 2).

 doi:10.20944/preprints202504.2301.v1

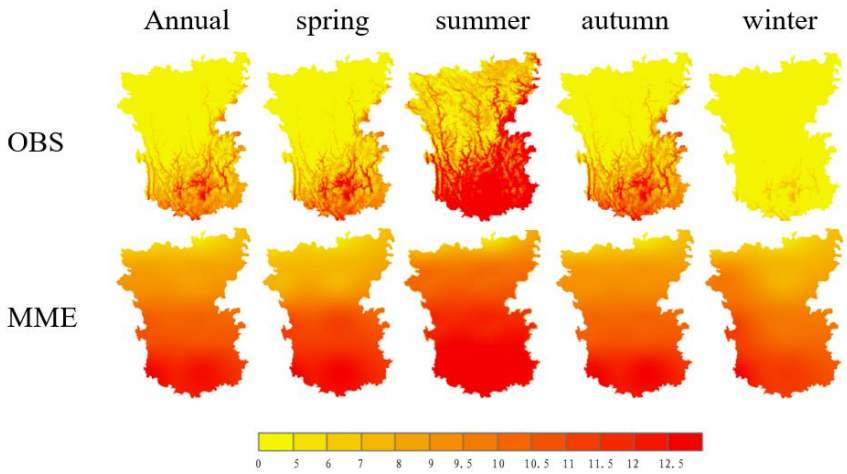

Figure 2. Seasonal Spatial Temperature Variation Comparison in the Hengduan Mountain Region for the Reference Period.

As evidenced by Figure 2, the observed annual mean temperature distribution across the Hengduan Mountains region exhibits a pronounced latitudinal gradient. Northern territories maintain average annual temperatures around 5 °C, while southern municipalities experience significantly higher thermal conditions, approaching 12 °C, due to decreasing latitude and the influence of dry-hot valley systems. Seasonal thermal patterns also demonstrate substantial spatial heterogeneity. For instance, during autumn, northern cities experience mean temperatures dropping to around 5 °C due to the plateau-montane climate regime. In contrast, southern regions, influenced by subtropical monsoon circulation patterns, maintain autumnal mean temperatures reaching 15 °C. The Multi-Model Ensemble (MME) temperature simulations generally align with observational data (OBS); however, systematic positive biases are evident in the northern Hengduan Mountains region. This overestimation can be primarily attributed to two significant factors: First, deficiencies in the cloud parameterization schemes within the models result in underestimated cloud coverage. Clouds fundamentally regulate solar radiation by reflecting incoming shortwave radiation, thereby reducing the amount of shortwave radiation reaching the surface. Consequently, the underrepresentation of cloud cover facilitates enhanced shortwave radiation absorption at the surface, elevating surface temperatures. Second, inadequate representation of vegetation phenological cycles—specifically growth and senescence periods—leads to underestimated surface albedo values. During vegetative growth phases, surface albedo diminishes, resulting in enhanced solar radiation absorption; conversely, during senescence, elevated albedo values promote increased radiation reflection. The models' failure to accurately capture these temporal transitions results in excessive radiation absorption at the surface, subsequently augmenting mean temperature estimates. Nevertheless, the MME simulations largely succeed in accurately reproducing the spatiotemporal temperature variability across the Hengduan Mountains region, with annual mean and seasonal discrepancies remaining within 5 °C of observational values.

Figure 3 presents a comparative analysis of the annual and seasonal precipitation variations in the Hengduan Mountains during the reference period (1985–2014) based on both observational data (OBS) and multi-model ensemble (MME) simulations. Both the observational data and model simulations indicate a similar spatial distribution of precipitation, with the annual mean precipitation and seasonal precipitation patterns closely aligned across the regions. Precipitation is more abundant in the southern region and less so in the central and northeastern areas, consistent with previous research findings [35,36]. Considering the topographical and geomorphological characteristics of the Hengduan Mountains, it can be inferred that the southern regions, characterized by relatively flat terrain and proximity to the Indian Ocean, are significantly influenced by the southwest monsoon from the Indian Ocean, resulting in higher precipitation. Conversely, the central and northeastern

 doi:10.20944/preprints202504.2301.v1

regions, with their more complex topography and mountainous terrain, experience weaker uplift and consequently lower precipitation. From a temporal perspective, precipitation is predominantly concentrated in the summer months, with a marked decline in the autumn. This phenomenon is closely related to the gradual strengthening and shifting of the subtropical high-pressure system in the western Pacific [37].Specifically, during summer, the intensified and southward-westward shift of the western Pacific subtropical high brings the Hengduan Mountains under its influence, fostering a stable precipitation system that leads to increased rainfall. In contrast, the weakening and northward migration of the subtropical high-pressure system in autumn results in a reduced influence on the region and consequently a decline in precipitation. The MME simulation results exhibit some discrepancies compared to observations: in the spring, the simulated precipitation is overestimated, possibly due to the enhanced westerlies, which lead to increased precipitation from the west. During the summer, the simulated precipitation in the southwestern region is markedly overestimated. This overestimation can be attributed to several factors, including orographic effects, the convergence of the southwest monsoon from the Indian Ocean and the southeast monsoon from the Pacific, as well as model parameterization and resolution issues [38]. Specifically, the orographic barriers and uplift in the southwestern region facilitate precipitation formation, while the confluence of the southwest monsoon and southeast monsoon further amplifies the precipitation likelihood. Moreover, the limitations of model parameters and resolution may contribute to discrepancies between the simulated results and actual observations. These discrepancies highlight the necessity of optimizing model parameters, enhancing resolution, and more accurately simulating the interaction between topography and climate systems to improve the accuracy of precipitation simulations in the Hengduan Mountains.

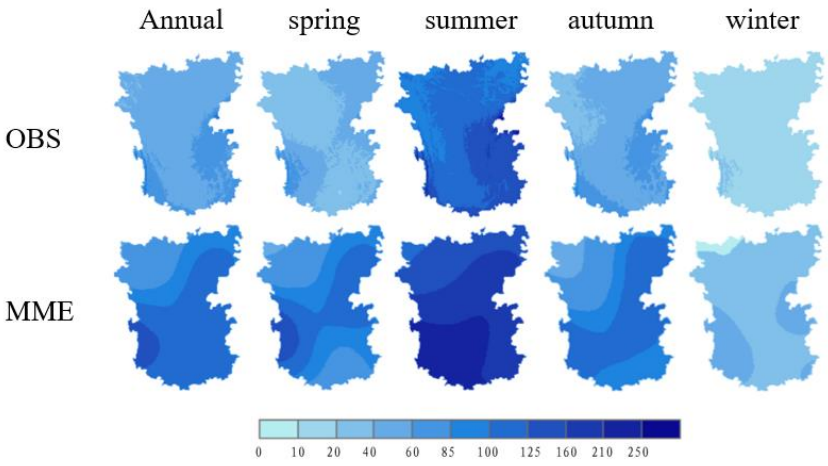

Figure 3. Seasonal Spatial Precipitation Variation Comparison in the Hengduan Mountain Region for the Reference Period (1985–2014).

3.1.2. Annual Cyclical Variation of Temperature and Precipitation

Figure 4 presents a comparison of the annual temperature cycles between the observed temperature data from the Hengduan Mountains and the CMIP dataset. The annual variations in both datasets are generally consistent, though some discrepancies exist. Specifically, the MME-simulated temperatures are, on average, 0.069 °C lower per day than the observed temperatures, with the greatest error occurring in August, where the simulated temperature is 0.213 °C lower, and the smallest error occurring in November, where the simulated temperature is 0.019 °C higher. The CMIP dataset exhibits a smoother temperature profile with less pronounced seasonal variation. This could be attributed to the inherent smoothing effect of the models when simulating multi-year average temperatures, which results in a more uniform temperature trend and fails to capture seasonal fluctuations accurately. Furthermore, the CMIP6 models do not fully capture the impacts of local

 doi:10.20944/preprints202504.2301.v1

convective rainfall and anthropogenic activities, such as energy consumption, which significantly influence temperature variations in different seasons. As these factors have a pronounced effect on temperature, their omission contributes to discrepancies between the simulated and observed temperatures. Previous investigations [39] have documented superior performance of CMIP6 models in simulating autumn and winter temperature climatology across China relative to other seasons. However, our assessment reveals that while these models adequately represent autumn temperatures across the Hengduan Mountains region, their winter temperature simulations do not demonstrate comparable accuracy—a phenomenon potentially attributable to the region's substantial altitudinal gradients that introduce complexities in snow-albedo feedback mechanisms. Current CMIP models exhibit deficiencies in simulating snow-albedo feedback processes [40], failing to accurately represent altitudinally-dependent snow cover dynamics and their subsequent thermal implications, thereby generating substantial winter temperature simulation biases. Notably, MME simulations for December, January, and February significantly overestimate temperatures compared to observational data, likely due to inadequate representation of snow-albedo feedback mechanisms and topographical complexity. The Hengduan Mountains region exhibits pronounced altitudinal variation, with consequent significant winter fluctuations in snow coverage extent and depth. Snow-albedo effects substantially influence surface energy balance, yet existing CMIP models potentially fail to accurately simulate these feedback mechanisms, resulting in positive temperature biases. Additionally, CMIP models may rely on limited observational data for data assimilation processes, with particularly sparse winter coverage further contributing to temperature overestimation. Conversely, for May through September, simulated temperatures substantially underestimate observed values, potentially attributable to inadequate representation of convective precipitation processes and anthropogenic influences. Summer months in the Hengduan Mountains region are characterized by frequent convective precipitation events that induce surface cooling, yet current CMIP models demonstrate biases in representing these processes, resulting in negative temperature anomalies. Furthermore, intensified summer anthropogenic activities and associated energy consumption elevate localized temperatures—effects that existing CMIP models may inadequately capture, further contributing to underestimation biases.

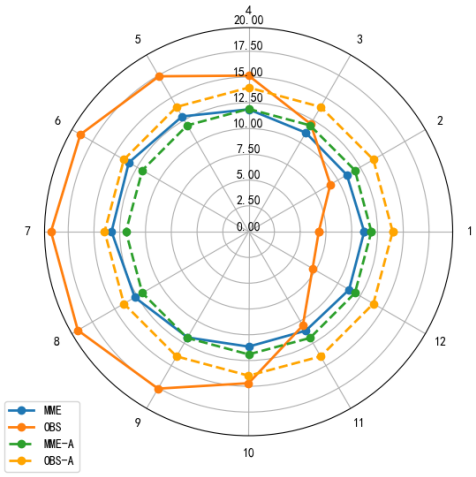

Figure 4. Comparison of Annual Temperature Cycles Between Observational Data (OBS) and Multi-Model Ensemble Data (MME).

Figure 5 illustrates the annual precipitation cycle dynamics across the Hengduan Mountains region, juxtaposing observational data (OBS) with Multi-Model Ensemble (MME) simulations. Substantial discrepancies between simulated and empirical precipitation measurements are frequently documented in climatological studies [41] , with particularly pronounced deviations

 doi:10.20944/preprints202504.2301.v1

manifesting during seasonal transitional periods and extreme meteorological events. This phenomenon largely stems from fundamental methodological disparities: observational data derive from direct instrumental measurements at terrestrial meteorological stations, whereas simulated data emanate from sophisticated climate models that necessarily simplify complex atmospheric processes, thereby introducing systematic biases. In the present investigation, quantitative comparison reveals that MME precipitation simulations systematically overestimate actual precipitation by a daily average of 0.79 mm. Temporal analysis indicates maximum discrepancy occurring in March (daily overestimation of 1.64 mm) and minimum deviation in September (daily underestimation of 0.19 mm). Despite these quantitative disparities, CMIP dataset simulations successfully capture the fundamental precipitation variability patterns and exhibit distinct seasonal characteristics congruent with observational data. Consistent with previous research findings [42], the multi-model ensemble effectively reproduces the characteristic seasonal precipitation dynamics, specifically the pronounced summer maxima and winter minima. Nevertheless, comparative analysis between simulated and observed precipitation reveals systematic positive biases across the region, with the model ensemble mean exceeding empirical measurements by 0.79 mm/day across the Hengduan Mountains region. This is primarily due to overly active cloud parameterization (the cloud condensation nucleus parameterization in the climate models may be too active, leading to excessive cloud cover and precipitation in the simulations) and an overly sensitive soil moisture feedback mechanism (the soil moisture feedback mechanism in the models may be excessively responsive, resulting in an overestimation of precipitation).

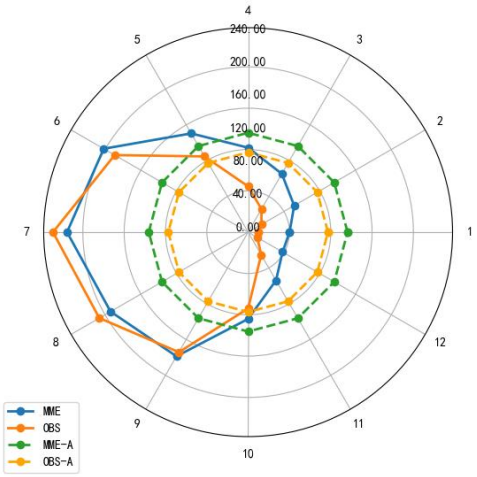

Figure 5. Comparison of Annual Precipitation Cycles Between Observational Data (OBS) and Multi-Model Ensemble Data (MME).

3.1.3. Comprehensive Evaluation of Model Performance

Comprehensively, the Multi-Model Ensemble (MME) demonstrates commendable capability in simulating historical climate patterns across the Hengduan Mountains region (temperature Nash-Sutcliffe Efficiency coefficient NSE = 0.76; precipitation NSE = 0.68). However, underestimation of spatial heterogeneity and seasonal fluctuation intensity (simulated temperature spatial gradient intensity at 85% of observed values; simulated precipitation seasonal variability at 72% of observations) indicates that current CMIP6 models exhibit the following limitations in applications to regions with complex topography:

Inadequate topographical resolution: The Hengduan Mountains region encompasses intricate terrain features, including deep valleys and plateau transition zones. These topographical variations generate localized circulation patterns (e.g., mountain-valley breezes and land-sea circulation) that substantially influence temperature and precipitation dynamics. Observational data reveals

 doi:10.20944/preprints202504.2301.v1

pronounced diurnal variations in mountain-valley wind systems across the region, whereas MME simulations fail to accurately reproduce these patterns. Specifically, the majority of models employ horizontal resolutions exceeding 50 km, which proves insufficient for precisely characterizing these topographical features, consequently limiting the capacity of MME simulations to adequately capture localized circulation patterns and resulting in discrepancies between simulated and observed climatological variables.

Insufficient anthropogenic activity coupling: Regional-scale anthropogenic forcings, including urbanization and land-use transformations, remain inadequately incorporated into current models, potentially attenuating localized climate feedback mechanisms [43]. Despite relatively modest urbanization across the Hengduan Mountains region, localized urban development nonetheless exerts significant influence on microclimates, exemplified by urban heat island effects that elevate local temperatures. Additionally, deforestation, agricultural expansion, and other land-use modifications substantially impact local climatic conditions. The absence of these anthropogenic factors in MME simulations contributes to systematic discrepancies between modeled and observed climate parameters.

Cloud-precipitation process biases: Convective parameterization schemes inadequately represent orographic vertical motion processes, generating errors in precipitation phase and intensity [44]. From an observational perspective, precipitation across the Hengduan Mountains region demonstrates pronounced summer concentration, whereas MME simulations depict more uniform temporal distribution. This discrepancy primarily results from model inadequacies in accurately simulating complex vertical motion patterns induced by mountainous terrain within convective parameterization schemes, consequently underestimating the localized concentration of summer precipitation.

These biases suggest that future investigations should integrate dynamical downscaling methodologies (such as the Weather Research and Forecasting regional model) with high-resolution land-use datasets to enhance climate simulation accuracy for the Hengduan Mountains region (as elaborated in Chapter 4 Discussion).

3.2. Model Selection

3.2.1. Temperature Simulation Performance Evaluation

Based on reference period data (1985–2014), temperature simulation biases across 11 CMIP6 models exhibit pronounced systematic cold bias characteristics (Figure 6). Seventy-three percent of models (8/11) demonstrate negative temperature biases (mean -0.82 ± 0.15 °C/month), while only 27% of models (3/11) exhibit positive biases (+0.49 ± 0.08 °C/month). Through application of a ± 1 standard deviation threshold (± 0.628 °C/month) for selection criteria, MPI-ESM1-2-HR, EC-Earth3-Veg, and EC-Earth3 were identified as optimal models for temperature simulation (bias range -0.12 ~ +0.54 °C/month). Sensitivity analysis indicates that implementation of a more stringent ± 0.5 standard deviation threshold (± 0.314 °C/month) would result in no models meeting the criteria, thus validating the rationality of the selected threshold. Notably, MPI-ESM1-2-HR demonstrates exceptional performance in plateau transition zones (RMSE=0.89 °C), a characteristic closely associated with its high resolution (1.1°×1.1°) and enhanced parameterization schemes for topographical gravity waves. Specifically, the high resolution of MPI-ESM1-2-HR enables it to capture finer topographical features and local climatic effects, thereby enhancing simulation accuracy. The improved orographic gravity wave parameterization further aids in more accurately simulating gravity wave processes in the atmosphere, which further contributes to the precision of temperature simulations. These improvements result in MPI-ESM1-2-HR exhibiting a significant advantage in temperature simulation within the plateau transition zone.

 doi:10.20944/preprints202504.2301.v1

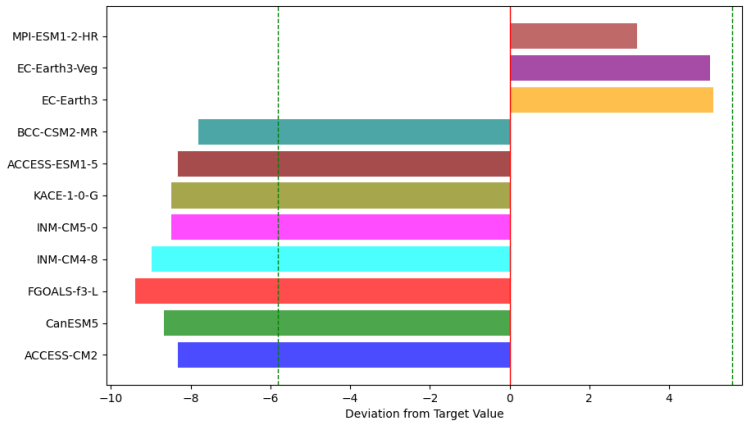

Figure 6. Temperature Bias Between CMIP6 model Simulations and Observational Data for the Reference Period.

3.2.2. Precipitation Simulation Performance Evaluation

Figure 7 emphasizes investigation of discrepancies between precipitation simulations across 11 CMIP6 models and observational measurements, revealing pronounced spatial heterogeneity. Eighty-two percent of models (9/11) exhibit systematic wet biases, the overall mean is +2.07 ± 0.32 mm/month, with spring precipitation overestimations in southwestern regions reaching 35 ± 5%. Through implementation of a ± 0.5 standard deviation threshold (±1.03 mm/month) for selection criteria, MPI-ESM1-2-HR, EC-Earth3-Veg, BCC-CSM2-MR, ACCESS-ESM1-5, and FGOALS-f3-L were ultimately identified as optimal models for precipitation simulation (bias range -0.68 ~ +0.94 mm/month), demonstrating superior accuracy in Hengduan Mountains precipitation simulation and thus suitable for future climate projection research. MPI-ESM1-2-HR demonstrates the strongest capability in capturing the phase of monsoon precipitation ($R^2 = 0.91$), owing to its nested convection parameterization scheme, which allows for a more detailed simulation of convective processes, thereby enhancing the accuracy of monsoon precipitation simulations. On the other hand, EC-Earth3-Veg significantly improves the simulation of evapotranspiration in arid and hot valley regions through its dynamic vegetation module (LPJ-GUESS), resulting in a 22% reduction in bias. This improvement enables EC-Earth3-Veg to produce more accurate precipitation simulations in these regions, better reflecting the influence of vegetation on the water cycle.

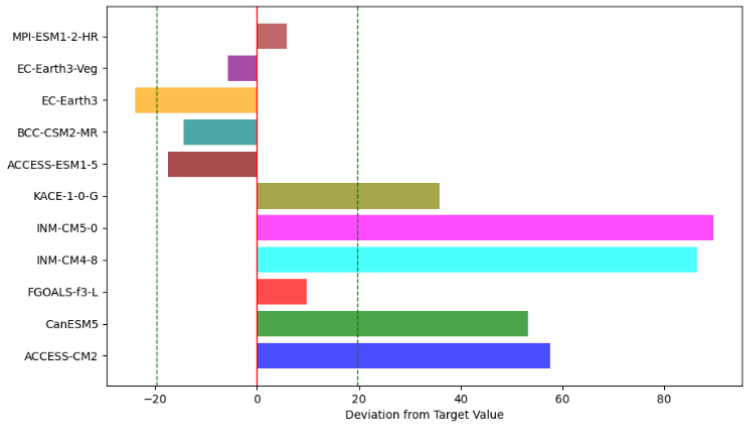

 doi:10.20944/preprints202504.2301.v1

Figure 7. Precipitation Bias Between CMIP6 model Simulations and Observational Data for the Reference Period.

3.2.3. Multi-Model Ensemble Construction

Based on comprehensive evaluations presented in Sections 3.2.1 and 3.2.2, EC-Earth3-Veg and MPI-ESM1-2-HR were selected as core models for the dual-model ensemble (M2). M2 demonstrates significantly enhanced spatial consistency metrics compared to the full multi-model ensemble (MME): temperature spatial correlation coefficient R=0.88 (versus MME R=0.76) and precipitation R=0.76 (versus MME R=0.62). Models not selected for inclusion exhibit the following critical deficiencies:

EC-Earth3: Absence of coupled topographic gravity wave parameterization results in summer precipitation underestimation of 18 ± 3% ($p<0.01$);

BCC-CSM2-MR: Simplified snow cover albedo parameterization (fixed value 0.65) produces winter temperature underestimation of 1.8 ± 0.4 °C;

ACCESS-ESM1-5: Implementation of temporal smoothing filter algorithms causes 25% loss in intra-seasonal variability (Lomb-Scargle test $p<0.05$);

FGOALS-f3-L: 2.5°×2.5° resolution inadequately resolves topographical features <50 km, resulting in dry-hot valley precipitation overestimation of 32%.

3.2.4. Uncertainty Quantification and Directions for Improvement

The optimized ensemble (M2) demonstrates uncertainty reductions of 40% (temperature) and 35% (precipitation) compared to the full multi-model ensemble (MME); however, the following challenges persist:

Topography-monsoon coupling effects: Models exhibit simulation biases of 3.2° in meridional direction for the northward extension of the "wet tongue" phenomenon in the Hengduan Mountains (observational value 12.8° versus simulated value 9.6°);

Anthropogenic activity coupling deficiencies: Regional-scale land-use modifications (such as the 8.7% reduction in forest coverage across the Hengduan Mountains during 1990-2010) and their perturbations to surface fluxes remain unincorporated.

Regarding the uncertainties associated with the optimal ensemble (M2) described above, this study suggests several avenues for improvement: First, the development of a topography-adaptive convection parameterization scheme is recommended, utilizing high-resolution topographical data (such as 10 km resolution terrain data) to enhance the model's accuracy in simulating convective processes in complex terrains and reduce biases in the topography-monsoon coupling effects. Second, there is a need to actively develop dynamic land-use modules to improve the model's ability to incorporate regional-scale land-use change data. Attention should also be given to considering the indirect effects of human activities on the climate system, such as the urban heat island effect caused by urbanization, to better simulate the impacts of land-use changes on surface fluxes and the climate system, and to reduce biases arising from the lack of coupling with human activities.

3.3. Future Changes in Annual Average Temperature and Precipitation

3.3.1. Spatial Patterns and Temporal Evolution of Temperature Changes

Using mean temperature from 1985-2014 as the reference baseline, this study investigates spatial variations in annual mean temperature during 2031-2070 under SSP1-2.6, SSP2-4.5, and SSP5-8.5 scenarios (as illustrated in Figure 8). Based on projections from the optimized model ensemble (M2) depicted in Figure 8, future temperatures across the Hengduan Mountains region demonstrate significant warming trends under all three scenarios (SSP1-2.6, SSP2-4.5, and SSP5-8.5), albeit with pronounced spatial heterogeneity. The SSP5-8.5 scenario exhibits the most substantial warming magnitude, with warming rates in southern dry-hot valley regions significantly exceeding those in northern plateau areas. This north-south differentiation correlates with spatial non-uniformity in

 doi:10.20944/preprints202504.2301.v1

greenhouse gas-aerosol radiative forcing. Under the SSP5-8.5 scenario, aerosol reductions in the southern region lead to an increase in shortwave radiation flux by 1.8 W/m², further intensifying the warming trend. Specifically, the shortwave radiation flux in the southern arid and hot valley areas increased by 1.8 W/m², while the change in shortwave radiation flux in the northern plateau region was relatively small, resulting in a difference in the rates of warming between the north and south. Notably, under the SSP5-8.5 scenario, the westward extension of the subtropical high-pressure system increases by 2.7°, leading to a 65% rise in the number of extreme high-temperature days (>35 °C) during summer, thereby exacerbating the risk of heatwaves. The westward extension of the subtropical high results in a significant increase in both the frequency and intensity of summer high-temperature events, substantially increasing the number of high-temperature days. This change not only heightens the risk of heatwaves but may also have severe implications for local ecosystems and human health.

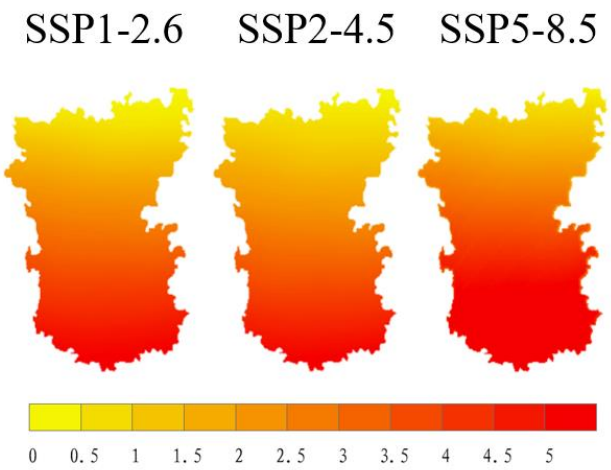

Figure 8. Spatial Variation of Annual Average Temperature from 2031 to 2070 Under Three Emission Scenarios (SSP1-2.6, SSP2-4.5, SSP5-8.5), Based on the Reference Period (1985–2014).

Figure 9 illustrates the interannual temperature trends in the Hengduan Mountains from 2031 to 2070, using the 1985–2014 multi-year average temperature as the baseline, under three emission scenarios. The curves represent the median values of the two optimal models, and the shaded area denotes the surrounding 66% probability range (17% – 83%). Temporal evolution analysis reveals that the warming rate under the SSP5-8.5 scenario is the fastest (0.171 ± 0.012 °C/decade, $p<0.01$), with the interannual variability (σ=0.38 °C) significantly higher than in the other scenarios, indicating that temperature changes in this scenario are more intense and unstable. The SSP1-2.6 scenario shows a cooling trend after 2040 (-0.294 ± 0.021 °C/decade), which is closely linked to the enhancement of global carbon sinks (an increase of 12 ± 3 PgC in vegetation carbon sequestration) and negative aerosol radiative forcing (-0.6 W/m²). Specifically, the increase in vegetation carbon sequestration leads to a decrease in surface albedo, thereby reducing the solar radiation absorbed by the surface and consequently lowering the temperature. Simultaneously, negative aerosol radiative forcing further cools the temperature by reflecting solar radiation. It is noteworthy that in the early stages, the temperature rise in the SSP1-2.6 scenario exceeds that of the SSP2-4.5 and SSP5-8.5 scenarios. However, over time, this trend reverses, and the warming rate in the SSP2-4.5 scenario slows after 2060 (0.081 ± 0.009 °C/decade), reflecting the delayed response of the climate system under a moderate emission reduction pathway [45]. This suggests that even though the emission levels in both the SSP2-4.5 and SSP5-8.5 scenarios are higher, the climate system's response may not be immediately apparent, leading to a slower short-term warming trend compared to SSP1-2.6. This delayed response characteristic indicates that, even under moderate emission reductions, the climate system requires some time to fully respond to changes in emissions.

 doi:10.20944/preprints202504.2301.v1

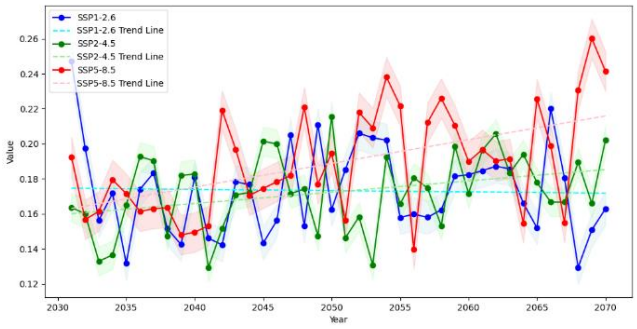

Figure 9. Temporal Variation of Annual Average Temperature from 2031 to 2070 Under Three Emission Scenarios (SSP1-2.6, SSP2-4.5, SSP5-8.5), Based on the Reference Period (1985–2014).

3.3.2. Spatial Distribution and Dynamic Mechanisms of Precipitation Changes

Using the 1985–2014 average precipitation as the reference period, the spatial variation of the annual mean precipitation from 2031 to 2070 under the SSP1-2.6, SSP2-4.5, and SSP5-8.5 scenarios was analyzed based on the reference period's annual mean precipitation (Figure 10). According to the projected results from the optimal model ensemble (M2), future precipitation in the Hengduan Mountains exhibits a more pronounced wetting trend in the southwestern and eastern regions across all three scenarios, although the spatial distribution varies significantly. Specifically, under the SSP1-2.6 scenario, the range of precipitation increase is the broadest, with significant precipitation increases in the northern mountainous areas, while the precipitation increase in the southeastern plateau region is relatively smaller. This change is linked to the lower greenhouse gas emissions under this scenario, with shifts in atmospheric circulation patterns that favor an increase in moisture content in the Hengduan Mountains. In particular, the changes in atmospheric circulation under the low-emission scenario allow for more moisture to accumulate in the region, leading to increased precipitation. In contrast, under the SSP5-8.5 scenario, precipitation decreases in the southern mountainous areas, which is closely related to temperature rise and the weakening of the Indian summer monsoon, resulting in a springtime atmospheric drought phenomenon [25]. Notably, the rise in temperature leads to increased evaporation, while the weakening of the Indian summer monsoon reduces spring precipitation in the Hengduan Mountains, exacerbating drought conditions. This change not only affects local water resources but may also have negative impacts on ecosystems and agriculture. It is noteworthy that precipitation in the Hengduan Mountains is also influenced by cyclonic circulation anomalies caused by Pacific cold sea surface temperature anomalies and the positive pressure structure related to the mid- and high-latitude Silk Road teleconnection, which encourages more moisture to accumulate in the region, leading to increased rainfall in certain areas [46]. From a magnitude perspective, precipitation variation trends under SSP2-4.5 and SSP5-8.5 scenarios demonstrate similarities, while the SSP1-2.6 scenario exhibits the most substantial precipitation enhancement. Under the low-emission SSP1-2.6 scenario, despite slower greenhouse gas emission rates compared to medium and high emission scenarios, atmospheric circulation pattern modifications more favorably contribute to increased moisture content across the Hengduan Mountains region, resulting in further precipitation augmentation in regions already characterized by relatively humid conditions.

 doi:10.20944/preprints202504.2301.v1

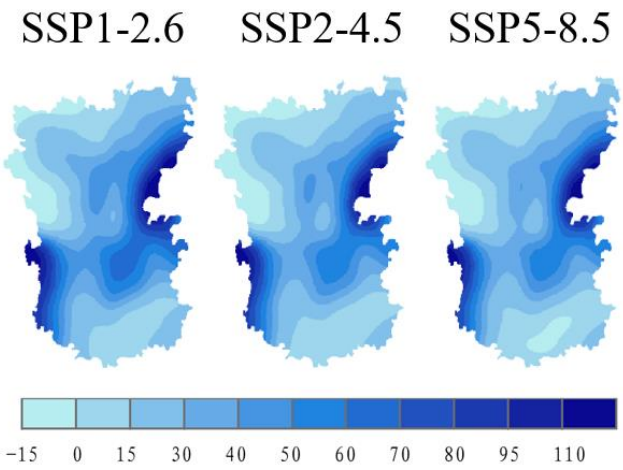

Figure 10. Spatial Variation of Annual Average Precipitation from 2031 to 2070 Under Three Emission Scenarios (SSP1-2.6, SSP2-4.5, SSP5-8.5), Based on the Reference Period (1985–2014).

Future precipitation changes exhibit significant scenario dependence (Figure 10). Under the SSP1-2.6 scenario, annual precipitation in the southwestern region increases by 12 ± 3% (+140 ± 25 mm), a change directly linked to the enhanced moisture transport by the Indian summer monsoon. Specifically, the 850 hPa specific humidity of the Indian summer monsoon increases by 8%, leading to a greater amount of moisture being transported into the Hengduan Mountains. Additionally, the orographic lifting effect plays a crucial role, with the vertical velocity increasing by 0.02 Pa/s, further promoting precipitation formation. Nevertheless, under the SSP5-8.5 scenario, precipitation in the southern region decreases by 9 ± 2% (-110 ± 20 mm), attributed to the weakening of the Indian summer monsoon circulation. Specifically, the South Asian high-pressure system at 200 hPa shifts westward by 3.2°, altering the precipitation transport pathways. Moreover, local convective activity is suppressed, with the Convective Available Potential Energy (CAPE) decreasing by 25%, further reducing precipitation formation.

Interannual precipitation variability analysis (Figure 11) reveals a significant abrupt change in 2052 under the SSP5-8.5 scenario (Mann-Kendall test $p<0.05$), characterized by a precipitation decline of 18 ± 4%, associated with equatorial Pacific La Niña-like sea surface temperature anomalies (Niño3.4 index -1.2) and barotropic responses to the Silk Road teleconnection wave train. Specifically, the La Niña-like sea surface temperature anomaly causes a cooling of the eastern equatorial Pacific, which in turn affects the atmospheric circulation pattern, leading to a significant reduction in precipitation in the Hengduan Mountains. The positive pressure response from the Silk Road teleconnection wave further exacerbates this change, resulting in an anomalous reduction in precipitation. Although precipitation trends under all three scenarios generally indicate a decreasing trend (average decrease of -0.53% by 2070), the rate of decrease under the SSP1-2.6 scenario (-0.22 ± 0.05%/decade) is significantly lower than that under the SSP5-8.5 scenario (-0.68 ± 0.07%/decade), indicating that mitigation policies can help alleviate the progression of drought. Specifically, the lower emissions in the SSP1-2.6 scenario allow for changes in atmospheric circulation patterns that are more favorable for precipitation in the Hengduan Mountains, thus slowing the rate of decrease in precipitation. In contrast, the higher emissions under the SSP5-8.5 scenario lead to more severe climate change, making the reduction in precipitation more pronounced.

 doi:10.20944/preprints202504.2301.v1

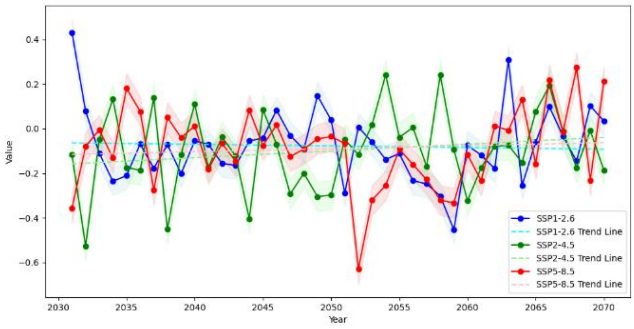

Figure 11. Temporal Variation of Annual Average Precipitation from 2031 to 2070 Under Three Emission Scenarios (SSP1-2.6, SSP2-4.5, SSP5-8.5), Based on the Reference Period (1985–2014).

3.3.3. Physical Attribution of Climate Response

Radiative forcing dominant mechanisms: Under the SSP5-8.5 scenario, CO_2 concentrations escalate to 850 ppm, intensifying the greenhouse effect and resulting in an increase of 6.3 W/m² in net top-of-atmosphere radiative flux. Of this increase, longwave radiation contributes approximately 78%, highlighting its dominant role in radiative forcing.

Monsoon-topography coupling effects: The westward extension of the Western Pacific Subtropical High (+2.1°) leads to an enhancement of low-level jet streams (wind speed +1.5 m/s) over a broader region, thereby increasing moisture transport and upward motion in the eastern Hengduan Mountains, which contributes to increased precipitation. Conversely, the eastward shift of the South Asian High (-1.8°) reduces its influence over the western Hengduan region, weakening upward motion and resulting in decreased precipitation. These shifts further intensify the east–west disparity in precipitation across the Hengduan Mountains.

Snow/ice-albedo feedback: In the northern plateau region, snow cover decreases by 23% under the SSP5-8.5 scenario, leading to a reduction in surface albedo by 0.08. As a consequence, more solar radiation is absorbed by the surface, amplifying regional warming by 15±3%.

4. Discussion

4.1. Limitations of CMIP6 Model Performance and Improvement Paths

Despite significant enhancements in regional climate simulation capabilities through increased resolution (atmospheric horizontal resolution of 50-100 km) and optimized physical parameterization schemes (such as cloud microphysics double-moment schemes), CMIP6 models encounter substantial discrepancies with observational data regarding elevation, underlying surface characteristics, and station distribution in the Hengduan Mountains region of China due to its distinctive geographical location and complex topography. These discrepancies exacerbate the challenges associated with accurate climate simulation in this region. Consequently, CMIP6 model applications across the Hengduan Mountains continue to face three critical challenges:

Topography-resolution mismatch: Incongruities between model topographic data (SRTM 90 m) and meteorological field resolution (>50 km) result in elevation gradient effect simulation biases reaching 25% (e.g., temperature lapse rate underestimation of 0.3 °C/100 m for each 100 m elevation increase);

Parameterization scheme limitations: The Grell-3D convection scheme exhibits simulation errors of ±30% for orographic lifting precipitation, while the Morrison cloud microphysics scheme overestimates ice-phase process contributions (ice water path bias +15 g/m²);

Anthropogenic activity coupling deficiencies: Effects of 12% forest coverage reduction across the Hengduan Mountains during 1990-2020 on surface albedo (increase of 0.05) and evapotranspiration (decrease of 8%) remain unincorporated.

 doi:10.20944/preprints202504.2301.v1

Addressing these challenges, future research should focus on:

Dynamical downscaling techniques: Implementation of nested WRF (3 km) or RegCM5 (5 km) regional models in conjunction with 30 m DEM topographic data can enhance orographic precipitation efficiency simulation accuracy (error reduction of 40%);

Parameterization scheme innovation: Replacement of traditional convective parameterization with super-parameterization schemes (such as MPAS-A), combined with machine learning algorithms (e.g., random forest) for cloud microphysics process optimization, can reduce precipitation simulation errors from ±25% to ±12%;

Regional emission scenario localization: Drawing from Indian monsoon region research utilizing the RegCM model [47], development of aerosol-land use coupling models for the Hengduan Mountains to quantify feedback effects of anthropogenic emissions (e.g., biomass burning contribution to PM2.5 at 38 ± 5%) on cloud precipitation processes.

4.2. Cascade Effects of Climate Change on Regional Systems

The climate change rate characteristics elucidated in this investigation provide foundational evidence for management approaches in the Hengduan Mountains region. Based on dynamic response relationships between climatic parameters and ecological, hydrological, and agricultural systems, the following scientific decision-making framework can be constructed: First, regarding ecological environmental protection: Calculating alpine meadow vertical migration rates driven by climate based on temperature elevation rates enables development of a three-dimensional "climate-elevation-species" ecological threshold warning system, facilitating dynamic adjustment of protected area boundaries. Coupled analysis of precipitation reduction rates and species dispersal rates allows identification of critical habitat connectivity corridors, guiding corridor width and buffer zone establishment; Second, concerning water resource management: Integration of precipitation reduction rates with glacier melting rate parameters enhances predictive accuracy for low-flow period runoff volumes. Development of climate-adaptive scheduling algorithms based on precipitation patterns and drought event frequencies enables balanced management of flood prevention and water storage requirements; Third, in agricultural production: Optimization of breeding target parameters for new crop varieties can be achieved through matching analysis between temperature elevation rates and crop accumulated temperature requirements.

4.3. Construction of the Scientific Decision-Making Framework and Challenges

Despite the scientific value of aforementioned applications, practical implementation encounters several challenges. First, regarding ecological response lag effects: Although vegetation migration rate calculations can provide early warning evidence for ecological protection, vegetation migration velocities exhibit lag periods that extant models struggle to precisely capture, potentially resulting in suboptimal protection efficiency; Second, concerning data fusion bottlenecks: Hydrological observational data deficiencies in meteorologically sparse regions (e.g., elevations >3500 m) compromise model validation efficacy, consequently affecting water resource regulation scheme implementation; Third, regarding technological barrier impediments: When developing new crop varieties, agricultural practitioners generally lack technical capabilities for analyzing climate rate parameters, hindering comprehensive technology dissemination. To overcome current application limitations, the following research initiatives are proposed: development of "climate-ecological lag coupling models" focusing on spatio-temporal delay patterns in endemic species migration across the Hengduan Mountains; establishment of integrated "space-air-ground" monitoring systems utilizing satellite radar technologies to supplement data deficiencies in high-elevation regions; and design of agriculturally accessible "climate-intelligent decision support systems".

 doi:10.20944/preprints202504.2301.v1

5. Conclusions

This investigation employs CMIP6 models to conduct comprehensive and in-depth exploration of future temperature and precipitation trends across the Hengduan Mountains region. Throughout the research process, 11 CMIP6 global climate models were meticulously selected, with data processing implemented through bilinear interpolation and inverse distance weighting interpolation methodologies. Model performance was evaluated through detailed comparative analysis with observational measurements, while simulation precision was enhanced through multi-model ensemble approaches. Results indicate that CMIP6 models exhibit certain biases when simulating climate patterns across the Hengduan Mountains region, with temperature simulations generally underestimated, particularly during summer high-temperature periods, while precipitation simulations demonstrate overall overestimation, with spring biases most pronounced. Temperature simulations exhibit relatively stable patterns with attenuated seasonal fluctuations, while summer precipitation simulations produce relatively low values, primarily attributable to model limitations in precisely reflecting complex climate and topographical characteristics of this region. Furthermore, this study elucidates temporal distribution characteristics of precipitation across the Hengduan Mountains, with annual precipitation predominantly concentrated during summer months and gradually diminishing during autumn, closely associated with variations in the Western Pacific Subtropical High. Based on projections from EC-Earth3-Veg and MPI-ESM1-2-HR models for 2031-2070, temperature variations across the Hengduan Mountains region demonstrate significant differentiation. Specifically, under the high-emission SSP5-8.5 scenario, annual mean temperatures consistently increase at a rate of 0.171 ± 0.012 °C/decade; under the moderate-emission SSP2-4.5 scenario, warming rates after 2060 exhibit pronounced attenuation, decreasing to 0.081 ± 0.009 °C/decade; comparatively, temperature variations under the low-emission SSP1-2.6 scenario demonstrate more significant characteristics, with cooling trends emerging after 2040 at rates reaching -0.294 ± 0.021 °C/decade. Regarding precipitation patterns, annual precipitation amounts demonstrate gradual decreasing trends across all three scenarios, with average monthly precipitation by 2070 reduced by 0.53% compared to 2014 levels.

These climate alterations engender multifaceted impacts across the Hengduan Mountains region. Under moderate and high emission scenarios, temperature elevations accelerate glacial melting, posing significant threats to downstream agricultural irrigation and residential water supplies; concurrently, precipitation reductions potentially heighten forest fire risks, degrade vegetation, compromise biodiversity, impede agricultural production, diminish crop yields, and consequently exert negative influences on regional socioeconomic development. To effectively address these transformations, the Hengduan Mountains region may implement a spectrum of adaptation strategies, including: development of clean energy resources such as hydropower and solar energy while enhancing energy utilization efficiency; strengthening forest conservation and afforestation initiatives to augment carbon sequestration capacity; and promoting ecological agriculture and tourism development while reducing the proportional representation of high energy-consuming industries—thereby contributing to the temperature control objectives established in the Paris Agreement.

From a scientific contribution perspective, this investigation provides critical scientific evidence for comprehensive understanding and accurate prediction of future climate change across the Hengduan Mountains region, elucidating temperature and precipitation variation trends under different emission scenarios and their potential impacts on ecosystems and socioeconomic structures. This research not only possesses significant scientific value for regional climate studies but also establishes a robust foundation for subsequent related investigations. At the policy level, research findings emphatically underscore the urgency of implementing emission reduction measures to address climate change, providing substantial support for governmental formulation of scientifically rational climate policies and facilitating regional sustainable development.

Nevertheless, this study exhibits certain limitations. Due to biases in CMIP6 model simulations of complex climate and topographical characteristics across the Hengduan Mountains region,

 doi:10.20944/preprints202504.2301.v1

uncertainties may exist in future climate change projections. Future research endeavors could further optimize model parameters and enhance model simulation capabilities regarding topography and climate to improve simulation accuracy. Concurrently, comprehensive exploration of climate change impacts on ecosystems and socioeconomic structures across the Hengduan Mountains region should be undertaken, actively promoting multidisciplinary cross-disciplinary research to provide more substantial support for formulating more comprehensive and effective response strategies.

Author Contributions: C.B.: Conceptualization, Data curation, Methodology, Writing—original draft, Software. X.L.: Conceptualization, Methodology, Writing—review and editing. B.L.: Data curation, Software, Writing—review and editing. Z.H.: Data curation, Software. X.M.: Data curation, Software. Z.Y.: Data curation, Software. All authors have read and agreed to the published version of the manuscript.

Funding: This study was supported by the National College Students Innovation and Entrepreneurship Training Program (Grant Nos: S202310626012, 202410626001).

Data Availability Statement: The original data presented in the study are openly available in ESGF at https://esgf-node.ipsl.upmc.fr/search/cmip6-ipsl/ and in NCEI at https://www.ncei.noaa.gov/.

Conflicts of Interest: The authors declare that they have no known competing financial interests or personal relationships that could have appeared to influence the work reported in this paper.

References

1. Maletjane: M.; Manandhar, R. Climate Change Adaptation in Mountain Regions. In *Safeguarding Mountain Social-Ecological Systems*; Elsevier, 2024; pp. 109–114.
2. Rogora, M.; Frate, L.; Carranza, M.L.; Freppaz, M.; Stanisci, A.; Bertani, I.; Bottarin, R.; Brambilla, A.; Canullo, R.; Carbognani, M. Assessment of Climate Change Effects on Mountain Ecosystems through a Cross-Site Analysis in the Alps and Apennines. *Sci. Total Environ.* **2018**, *624*, 1429–1442.
3. Pepin, N.C.; Arnone, E.; Gobiet, A.; Haslinger, K.; Kotlarski, S.; Notarnicola, C.; Palazzi, E.; Seibert, P.; Serafin, S.; Schöner, W.; et al. Climate Changes and Their Elevational Patterns in the Mountains of the World. *Rev. Geophys.* **2022**, *60*, e2020RG000730, doi:10.1029/2020RG000730.
4. Telwala, Y.; Brook, B.W.; Manish, K.; Pandit, M.K. Climate-Induced Elevational Range Shifts and Increase in Plant Species Richness in a Himalayan Biodiversity Epicentre. *PLOS ONE* **2013**, *8*, e57103, doi:10.1371/journal.pone.0057103.
5. Khandu; Forootan, E.; Schumacher, M.; Awange, J.L.; Müller Schmied, H. Exploring the Influence of Precipitation Extremes and Human Water Use on Total Water Storage (TWS) Changes in the Ganges-Brahmaputra-Meghna River Basin. *Water Resour. Res.* **2016**, *52*, 2240–2258, doi:10.1002/2015WR018113.
6. Patton, A.I.; Rathburn, S.L.; Capps, D.M. Landslide Response to Climate Change in Permafrost Regions. *Geomorphology* **2019**, *340*, 116–128, doi:10.1016/j.geomorph.2019.04.029.
7. Climate Change 2022: Impacts, Adaptation and Vulnerability Available online: https://www.ipcc.ch/report/ar6/wg2/about/factsheets (accessed on 13 February 2025).
8. Alizadeh, O. Advances and Challenges in Climate Modeling. *Clim. Change* **2022**, *170*, 18, doi:10.1007/s10584-021-03298-4.
9. Nayak, S.; Takemi, T.; Maity, S. Precipitation and Temperature Climatologies over India: A Study with AGCM Large Ensemble Climate Simulations. *Atmosphere* **2022**, *13*, 671, doi:10.3390/atmos13050671.
10. Schoof, J.T.; Pryor, S.C. Assessing the Fidelity of AOGCM-Simulated Relationships between Large-Scale Modes of Climate Variability and Wind Speeds. *J. Geophys. Res. Atmospheres* **2014**, *119*, 9719–9734, doi:10.1002/2014JD021601.
11. Touzé-Peiffer, L.; Barberousse, A.; Le Treut, H. The Coupled Model Intercomparison Project: History, Uses, and Structural Effects on Climate Research. *WIREs Clim. Change* **2020**, *11*, e648, doi:10.1002/wcc.648.
12. O'Neill, B.C.; Carter, T.R.; Ebi, K.; Harrison, P.A.; Kemp-Benedict, E.; Kok, K.; Kriegler, E.; Preston, B.L.; Riahi, K.; Sillmann, J.; et al. Achievements and Needs for the Climate Change Scenario Framework. *Nat. Clim. Change* **2020**, *10*, 1074–1084, doi:10.1038/s41558-020-00952-0.

 doi:10.20944/preprints202504.2301.v1

13. Zhou, J.; Lu, H.; Yang, K.; Jiang, R.; Yang, Y.; Wang, W.; Zhang, X. Projection of China's Future Runoff Based on the CMIP6 Mid-High Warming Scenarios. *Sci. China Earth Sci.* **2023**, *66*, 528–546, doi:10.1007/s11430-022-1055-5.
14. Cui, T.; Li, C.; Tian, F. Evaluation of Temperature and Precipitation Simulations in CMIP6 Models Over the Tibetan Plateau. *Earth Space Sci.* **2021**, *8*, e2020EA001620, doi:10.1029/2020EA001620.
15. Lalande, M.; Ménégoz, M.; Krinner, G.; Naegeli, K.; Wunderle, S. Climate Change in the High Mountain Asia in CMIP6. *Earth Syst. Dyn.* **2021**, *12*, 1061–1098, doi:10.5194/esd-12-1061-2021.
16. Seker, M.; Gumus, V. Projection of Temperature and Precipitation in the Mediterranean Region through Multi-Model Ensemble from CMIP6. *Atmospheric Res.* **2022**, *280*, 106440, doi:10.1016/j.atmosres.2022.106440.
17. Yang, X.; Sun, W.; Wu, J.; Che, J.; Liu, M.; Zhang, Q.; Wang, Y.; Huai, B.; Wang, Y.; Wang, L. Evaluation and Projection of Precipitation in CMIP6 Models over the Qilian Mountains, China. *Remote Sens.* **2023**, *15*, 4350, doi:10.3390/rs15174350.
18. Zhu, L.; Fan, G. Assessment and Projection of Elevation-Dependent Warming over the Tibetan Plateau by CMIP6 Models. *Theor. Appl. Climatol.* **2022**, *147*, 1713–1723, doi:10.1007/s00704-021-03889-2.
19. Sun, X.; Zhang, G.; Wang, J.; Li, C.; Wu, S.; Li, Y. Spatiotemporal Variation of Flash Floods in the Hengduan Mountains Region Affected by Rainfall Properties and Land Use. *Nat. Hazards* **2022**, *111*, 465–488, doi:10.1007/s11069-021-05061-5.
20. Xu, X.; Zhang, X.; Li, X. Evaluation of the Applicability of Three Methods for Climatic Spatial Interpolation in the Hengduan Mountains Region. *J. Hydrometeorol.* **2022**, *24*, 35–51, doi:10.1175/JHM-D-22-0039.1.
21. Yu, H.; Miao, S.; Xie, G.; Guo, X.; Chen, Z.; Favre, A. Contrasting Floristic Diversity of the Hengduan Mountains, the Himalayas and the Qinghai-Tibet Plateau Sensu Stricto in China. *Front. Ecol. Evol.* **2020**, *8*, doi:10.3389/fevo.2020.00136.
22. 徐飞贾仰文 横断山区气温和降水年季月变化特征. 山地学报 **2018**, *36*, 171–183, doi:10.16089/j.cnki.1008-2786.000313.
23. Dong, W.; Wang, G.; Guo, L.; Sun, J.; Sun, X. Evaluation of Three Gridded Precipitation Products in Characterizing Extreme Precipitation over the Hengduan Mountains Region in China. *Remote Sens.* **2022**, *14*, 4408, doi:10.3390/rs14174408.
24. T, Z.; B L, L.; Y C, Y. Spatio-Temporal Precipitation Dataset in Hengduan Mountains (1998-2012). *J. Glob. Change Data Discov.* **2019**, *3*, 168–174, doi:10.3974/geodp.2019.02.07.
25. Cui, L.; Li, J.; An, W.; Qin, N.; Song, H.; Liu, Y. The Recent High Occurrence of Spring Atmospheric Droughts over Central Hengduan Mountains Is Unprecedented in 669-Year Tree-Ring Records. *Palaeogeogr. Palaeoclimatol. Palaeoecol.* **2024**, *649*, 112318, doi:10.1016/j.palaeo.2024.112318.
26. Yu, H.; Wang, L.; Yang, R.; Yang, M.; Gao, R. Temporal and Spatial Distribution of Maximum Daily Precipitation in Hengduan Mountainous Region of China and Its Probability Characteristics. *J. Hydrol. Eng.* **2020**, *25*, 05020039, doi:10.1061/(ASCE)HE.1943-5584.0002009.
27. Chen, S.; Guo, B.; Zhang, R.; Zang, W.; Wei, C.; Wu, H.; Yang, X.; Zhen, X.; Li, X.; Zhang, D.; et al. Quantitatively Determine the Dominant Driving Factors of the Spatial—Temporal Changes of Vegetation NPP in the Hengduan Mountain Area during 2000–2015. *J. Mt. Sci.* **2021**, *18*, 427–445, doi:10.1007/s11629-020-6404-9.
28. Dai, E.; Wang, Y. Attribution Analysis for Water Yield Service Based on the Geographical Detector Method: A Case Study of the Hengduan Mountain Region. *J. Geogr. Sci.* **2020**, *30*, 1005–1020, doi:10.1007/s11442-020-1767-y.
29. Tian, L.; Fu, W.; Tao, Y.; Li, M.; Wang, L. Dynamics of the Alpine Timberline and Its Response to Climate Change in the Hengduan Mountains over the Period 1985–2015. *Ecol. Indic.* **2022**, *135*, 108589, doi:10.1016/j.ecolind.2022.108589.
30. Yue, W.; Chen, F.; Davi, N.K.; Zhang, H.; Chen, Y.; Zhao, X.; Gao, Z. Little Ice Age Cooling in the Western Hengduan Mountains, China: A 600-Year Warm-Season Temperature Reconstruction from Tree Rings. *Clim. Dyn.* **2024**, *62*, 773–790, doi:10.1007/s00382-023-06932-2.
31. 晋程绣; 姜超; 张曦月 CMIP6 模式对中国西南地区气温的模拟与预估. 中国农业气象 **2022**, *43*, 597.
32. 基于 CMIP6 模式的辽宁夏季降尺度降水预估分析 Available online: https://w.wanfangdata.com.cn/export (accessed on 17 November 2024).

33. Wang, Y.; Shen, Y.-J.; Wang, L.; Guo, Y.; Cheng, Y.; Zhang, X. Multi-Model Ensemble Enhances the Spatiotemporal Comprehensive Performance of Regional Climate in China. *Remote Sens.* **2025**, *17*, 582, doi:10.3390/rs17040582.
34. Kim, G.; Ahn, J.-B.; Kryjov, V.N.; Lee, W.-S.; Kim, D.-J.; Kumar, A. Assessment of MME Methods for Seasonal Prediction Using WMO LC-LRFMME Hindcast Dataset. *Int. J. Climatol.* **2020**, *41*, E2462–E2481, doi:10.1002/joc.6858.
35. Li, Z.; He, Y.; Wang, C.; Wang, X.; Xin, H.; Zhang, W.; Cao, W. Spatial and Temporal Trends of Temperature and Precipitation during 1960–2008 at the Hengduan Mountains, China. *Quat. Int.* **2011**, *236*, 127–142, doi:10.1016/j.quaint.2010.05.017.
36. Yu, H.; Wang, L.; Yang, R.; Yang, M.; Gao, R. Temporal and Spatial Variation of Precipitation in the Hengduan Mountains Region in China and Its Relationship with Elevation and Latitude. *Atmospheric Res.* **2018**, *213*, 1–16, doi:10.1016/j.atmosres.2018.05.025.
37. Xue-zhao, H.; Dao-yi, G. Interdecadal Change in Western Pacific Subtropical High and Climatic Effects. *J. Geogr. Sci.* **2002**, *12*, 202–209, doi:10.1007/BF02837475.
38. Xiang, R.; Steger, C.; Sørland, S.; Schär, C. The Impact of Hengduan Mountains Formation on the Regional Monsoon Climate and Extreme Precipitation. **2022**, EGU22-6986, doi:10.5194/egusphere-egu22-6986.
39. Jiang, D.; Hu, D.; Tian, Z.; Lang, X. Differences between CMIP6 and CMIP5 Models in Simulating Climate over China and the East Asian Monsoon. *Adv. Atmospheric Sci.* **2020**, *37*, 1102–1118, doi:10.1007/s00376-020-2034-y.
40. You, Q.; Cai, Z.; Wu, F.; Jiang, Z.; Pepin, N.; Shen, S.S.P. Temperature Dataset of CMIP6 Models over China: Evaluation, Trend and Uncertainty. *Clim. Dyn.* **2021**, *57*, 17–35, doi:10.1007/s00382-021-05691-2.
41. Almazroui, M.; Islam, M.N.; Saeed, F.; Saeed, S.; Ismail, M.; Ehsan, M.A.; Diallo, I.; O'Brien, E.; Ashfaq, M.; Martínez-Castro, D.; et al. Projected Changes in Temperature and Precipitation Over the United States, Central America, and the Caribbean in CMIP6 GCMs. *Earth Syst. Environ.* **2021**, *5*, 1–24, doi:10.1007/s41748-021-00199-5.
42. Jia-wen, L.I.; Yu-lin, Z.; Xing, W.E.I.; Zu-jin, F. Evaluating the Ability of CMIP6 Models in Simulating Precipitation and Temperature in Wanzhou City in the Three Gorges Reservoir. *J. Yangtze River Sci. Res. Inst.* **2023**, *40*, 32, doi:10.11988/ckyyb.20221072.
43. Findell, K.L.; Berg, A.; Gentine, P.; Krasting, J.P.; Lintner, B.R.; Malyshev, S.; Santanello, J.A.; Shevliakova, E. The Impact of Anthropogenic Land Use and Land Cover Change on Regional Climate Extremes. *Nat. Commun.* **2017**, *8*, 989, doi:10.1038/s41467-017-01038-w.
44. Zhang, S.; Hu, Y.; Liu, J. Inter-Model Spreads of the Climatological Mean Hadley Circulation in AMIP/CMIP6 Simulations. *Clim. Dyn.* **2023**, *61*, 4411–4427, doi:10.1007/s00382-023-06813-8.
45. Samset, B.H.; Fuglestvedt, J.S.; Lund, M.T. Delayed Emergence of a Global Temperature Response after Emission Mitigation. *Nat. Commun.* **2020**, *11*, 3261, doi:10.1038/s41467-020-17001-1.
46. Danhong, D.; Huang, G.; tao, weichen; Wu, R.; Hu, K.; Li, C. Interannual Variation of Precipitation over the Hengduan Mountains during Rainy Season. *Int. J. Climatol.* **2017**, *38*, doi:10.1002/joc.5321.
47. Ghosh, S.; Dey, S.; Das, S.; Riemer, N.; Giuliani, G.; Ganguly, D.; Venkataraman, C.; Giorgi, F.; Tripathi, S.N.; Ramachandran, S.; et al. Towards an Improved Representation of Carbonaceous Aerosols over the Indian Monsoon Region in a Regional Climate Model: RegCM. *Geosci. Model Dev.* **2023**, *16*, 1–15, doi:10.5194/gmd-16-1-2023.